NPG Asia Materials

ARTICLE Open Access

Biodegradable, flexible silicon nanomembrane-based NO_x gas sensor system with record-high performance for transient environmental monitors and medical implants

Gwan-Jin Ko[1], Soo Deok Han[2], Jeong-Ki Kim[1], Jia Zhu[3], Won Bae Han[1], Jinmook Chung[1], Seung Min Yang[1], Huanyu Cheng[3], Dong-Hwee Kim[1], Chong-Yun Kang[1,4] and Suk-Won Hwang[1]

Abstract

A novel transient electronics technology that is capable of completely dissolving or decomposing in certain conditions after a period of operation offers unprecedented opportunities for medical implants, environmental sensors, and other applications. Here, we describe a biodegradable, flexible silicon-based electronic system that detects NO species with a record-breaking sensitivity of 136 Rs (5 ppm, NO_2) and 100-fold selectivity for NO species over other substances with a fast response (~30 s) and recovery (~60 s). The exceptional features primarily depend on not only materials, dimensions, and design layouts but also temperatures and electrical operations. Large-scale sensor arrays in a mechanically pliable configuration exhibit negligible deterioration in performance under various modes of applied loads, consistent with mechanics modeling. In vitro evaluations demonstrate the capability and stability of integrated NO_x devices in severe wet environments for biomedical applications.

Introduction

Electronic materials and devices that are biologically benign or mechanically elastic have been utilized in versatile applications, including electronic skin (E-skin) and biomedicine, for the diagnosis and treatment of diseases due to their advantages of nontoxicity, bioresorption, and mechanical properties similar to those of human skin and organs. Published examples involve sweat-based analysis[1–3], epidermal virtual reality[4,5], self-healing electronics[6,7], optoelectronic elements[8,9], and neurorelated systems[10–13]. Although the technological advances in the corresponding areas delivered innovative output products, a relatively unexplored research opportunity exists in detectable species indicative of occurrences in organisms that may affect the prevalence and severity of human health, such as infections, injuries, diseases, or environmental exposures. One of the key signaling elements is nitric oxide (NO), which is produced naturally in the human body and plays an essential role in many aspects of maintaining health by relaxing or widening blood vessels to enhance blood flow, allowing nutrients, and oxygen to travel to every part of the human body[14,15]. In nonbiological cases, highly reactive nitric oxide can be transformed into nitrogen dioxide (NO_2) with other participants, contributing to acid rain deposition and harmful ozone generation[16,17]. Research approaches for NO species in previous works have explored high-performance channel materials such as graphene, carbon nanotubes, polymers, and metal oxides[18–20] or modifications to these structures for a high surface-to-volume ratio[21–25], while several issues, including rigidity, low sensitivity, poor

Correspondence: Chong-Yun Kang (cykang@kist.re.kr) or Suk-Won Hwang (dupong76@korea.ac.kr)
[1]KU-KIST Graduate School of Converging Science and Technology, Korea University, 145 Anam-ro, Seongbuk-gu, Seoul 02841, Republic of Korea
[2]Electrical Engineering Division, Department of Engineering, University of Cambridge, 9 JJ Thomson Avenue, Cambridge CB3 0FA, UK
Full list of author information is available at the end of the article
These authors contributed equally: Gwan-Jin, Soo Deok Han

selectivity, high power consumption, and nonbiodegradability, still need to be considered for wearable and implantable electronic systems. Here, we report a flexible and bioresorbable single-crystal silicon nanomembrane (SC-Si NM)-based NO_x sensing system operating at room temperature with exceptional sensitivity and selectivity. The results focus on detailed studies of electrical responses of Si NMs under various conditions, and of the mechanical properties of the electronic system with theoretical considerations. In vitro assessments that incorporate semipermeable membranes provide information on their potential applicability in disposable environmental monitors and bioresorbable medical implants.

Experimental procedure

Fabrication of a transient NO_x (NO/NO_2)-sensing system on various substrates

Device fabrication began with thinning down SC-Si NMs on silicon-on-insulator (SOI, SOITEC, France) wafers (top silicon ~300 nm in thickness). Repeated oxidation of SC-Si NMs at an elevated temperature (1100 °C) and removal of the thermally grown SiO_2 by wet etching with hydrofluoric acid (HF, 49%, J. T Baker, USA), allowed to reach a desired target thickness of Si NMs (~100 nm). Phosphorus doping at 950 °C with spin-on dopant (SOD, Filmtronics, USA) formed highly doped regions for electrical contacts of a NO_x sensing system. Undercut wet etching of box oxide released the thinned SC-Si NMs from the carrier wafers, enabling transfer printing onto a PMMA/diluted PI-coated temporary substrate. Active areas of the SC-Si NMs for NO_x gas, humidity, and temperature sensors were defined by sulfur hexafluoride (SF_6)-based reactive ion etching, followed by deposition of interdigitated electrodes (IDEs) with a layer of magnesium (Mg, ~300 nm) using an electron-beam (e-beam) evaporator (VER5004, SNTEK, Korea). Formations of patterned dielectric layers and contact pads were generated by wet etching using buffered oxide etchant (BOE, 6:1, J. T baker, USA) and e-beam evaporation. A geometry of mesh-typed bridges was employed to facilitate lifting off the device, enabling the release of the system from the temporary substrate. After removal of the bottom PI layer, the device was transfer printed onto degradable substrates for a complete transient electronic system.

Characterization of soft, biodegradable NO_x sensors

The electrochemical properties of a silicon-based gas detector were measured using an electrometer (Keithley 2636B) under a DC bias voltage of 0.01 V. Experiments were conducted in a temperature-adjustable chamber (RT ~50 °C, Lindberg, USA) with a constant flow rate of 1000 sccm controlled by mass flow controllers (MFCs). Electrical responses of sensors were determined by measurements of baseline resistances in dry N_2/air and saturated resistances after exposure to target gases for 500 s. The responses to reducing and oxidizing gases were defined as R_0/R_{gas} and R_{gas}/R_0, where R_{gas} and R_0 denote the resistances of the target gases and dry N_2/air, respectively.

Cell culture and M1 activation

RAW 264.7 cells were cultured in Dulbecco's modified Eagle's medium (DMEM) supplemented with 10% fetal bovine serum (FBS), 100 U/ml penicillin, and 100 μg/ml streptomycin. Cells were incubated at 37 °C with 5% CO_2 in a humidified incubator. To induce M1 activation, 100 ng/ml LPS (lipopolysaccharide, Sigma) and 20 ng/ml IFN-γ (interferon-gamma, Peprotech) were added to the culture medium, and it was incubated for 24 h.

DAF-FM assay for NO measurement

After M1 activation, cells were incubated in L-arginine-free DMEM (Thermo, 88364) for 30 min, collected using a cell scraper and replated in 48-well plates. To measure NO production in cells, 10 μM DAF-FM DA (Sigma, D1946) was added to medium with or without 150 μM L-arginine, and the system was incubated for 30 min. The fluorescence intensity of DAF-FM-stained cells was measured using a Cytation 3 Cell Imaging Multi-Mode Reader (Bio-Tek).

Immunofluorescence microscopy

Cells were fixed using 4% paraformaldehyde for 10 min at 4 °C and permeabilized with 0.05% Triton X-100 for 5 min. After blocking with FBS (10%, v/v)-supplemented PBS for 30 min, cells were incubated with anti-iNOS antibody (1:500, Abcam, ab178945) for 60 min. Cells were then incubated with secondary antibodies (1:500, Bethyl, A120-100D4) for 60 min in the dark. The nucleus and F-actin were stained with DAPI (Invitrogen) and Alexa Fluor phalloidin (1:50, Invitrogen, A12379), respectively. The fluorescence confocal images were captured using confocal laser microscopy (A1R, Nikon) through a ×60 oil immersion objective (N.A. 1.4).

Detection of NO_x produced in M1-activated cells

M1-activated cells were transferred into a sterile cell-culture flask containing 2 ml L-arginine-free DMEM. NO sensors were placed into the flask, and L-arginine was provided through needles embedded in stoppers. The NO sensors were connected with ACF cables to an electrometer, and all measurements were recorded through LabVIEW with the GPIB interface.

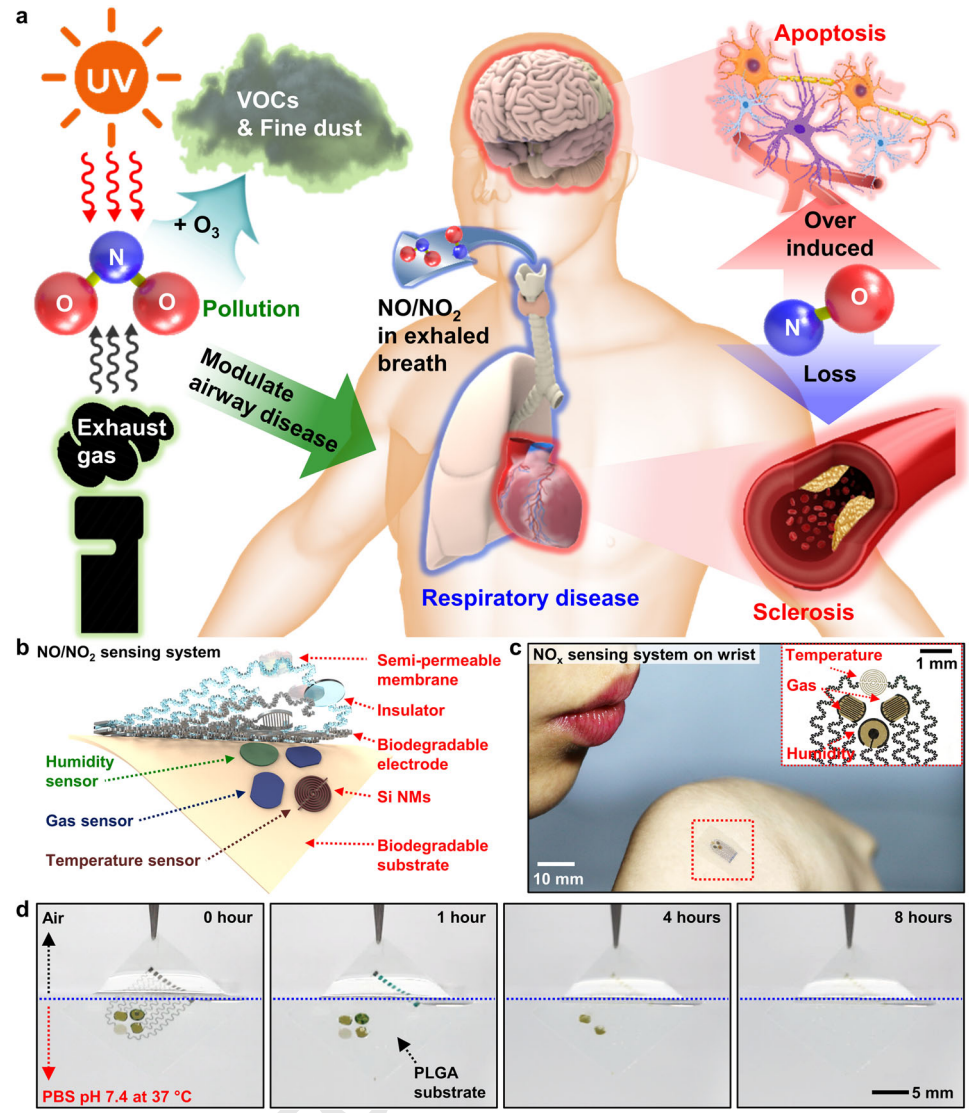

Fig. 1 Bioresorbable, flexible NO_x (NO/NO_2) sensing system based on single crystalline silicon nanomembranes (SC-Si NMs). Illustration of a variety of crucial environmental and biological phenomena and effects induced by NO_x. **b** Schematic exploded view of a NO_x sensing system including gas, temperature and humidity sensors on biodegradable polymer substrates. **c** Optical micrograph of a representative sensor system laminated on a wrist, with a magnified view of the device in the inset. **d** Images collected at sequential stages of dissolution of the NO_x-based sensor system initiated by immersion in an aqueous buffer solution (pH 7.4) at room temperature.

Results and discussion

Integrated bioresorbable, flexible NO_x (NO/NO_2) sensing system

Figure 1a illustrates the examples of various adverse environmental and biological effects that may be caused by nitrogen oxides (NO_x). NO has been well recognized as a biomarker for nervous, vascular, and respiratory systems[26–28] and a major air pollutant giving rise to acid rain and ozone generation after transformation into NO_2 as a reaction intermediate. Figure 1b provides an exploded view drawing of a soft, bioresorbable NO_x sensing system that includes highly sensitive and selective silicon nanomembrane (Si NM)-based gas sensors at room temperature and a temperature and hydration monitor to adjust the properties of the gas sensors affected by those parameters. The electronic system consists of patterned single-crystal silicon nanomembranes (SC-Si NMs, thickness ~100 nm) doped with phosphorous using spin-on dopant (SOD, Filmtronics) for reactive materials, magnesium (Mg, thickness ~300 nm) as electrodes, silicon dioxide (SiO_2, thickness ~100 nm) as interlayer dielectric, and an elastomeric polymer (PDMS, thickness ~20 μm) as a semipermeable membrane to maintain a stable gas sensing performance in humid and wet conditions.

Sample preparation involves thinning of SC-Si NMs to a targeted value (~100 nm), doping with phosphorous at selected regions on silicon-on-insulator (SOI) wafers and transfer printing doped SC-Si NMs to a temporary foreign substrate. Electrodes and insulators were evaporated and patterned through deposition, photolithography and etching, and transfer printing of the resulting components to a biodegradable substrate completed the whole process. In the case of measurements in humid or wet conditions, facile spin casting of PDMS was applied to the obtained sample to form a gas-permeable membrane. The bioresorbable, flexible NO_x sensing system laminated on a wrist appears in Fig. 1c, with a magnified image of the individual gas, temperature, and humidity sensors in the inset (more images in Fig. S1). Figure 1d shows a set of images of the temporal degradation behavior of a representative NO_x sensing system assembled on a poly(lactic-co-glycolic) acid (PLGA) substrate during half-immersion in a PBS (pH 7.4) at 37 °C for 0, 1, 4, and 8 h. All constituent materials dissolved via hydrolysis to form nontoxic end products. Mg electrodes, with a relatively rapid dissolution rate, disappeared faster than other components via the reaction $Mg + 2H_2O \rightarrow Mg(OH)_2 + H_2$, and SC-Si NMs, SiO_2, and PLGA gradually dissolved at rate similar to previously reported dissolution rates while undergoing the reactions $Si + 4H_2O \leftrightarrow Si(OH)_4 + 2H_2$, $SiO_2 + 2H_2O \rightarrow Si(OH)_4$, and poly(lactic-co-glycolic acid) → lactic acid + glycolic acid + H_2[29–31]. Additional dissolution images at different stages appear in Fig. S2.

Q4

High-performance biodegradable NO_x sensing system based on silicon nanomembranes

Figure 2a illustrates the fundamental mechanism of SC-Si NMs reacting with nitrogen oxides. Changes in the electrical properties of *n*-type semiconductor sensors resulted from variations in a depletion layer on the surface through adsorption and reaction with the oxidizing gas molecules, i.e., electrons were extracted from the SC-Si NMs as the reaction NO_x (gas) + e^- → NO_x^- (ads) occurred. Figure 2b represents a measured response to 5 ppm of NO_2 at room temperature (RT) with a superb sensitivity of 136 Rs (13,600%) as well as fast response (30 s) and recovery (60 s) rates, which surpass those of previously reported room-temperature sensors based on various materials, including carbon nanotubes (1.14–1.2 Rs), graphene (1.12–1.6 Rs), polymers (5 Rs) and metal oxides (2.2 Rs), and a commercial gas sensor (7 Rs, MICS-2714, Amphenol SGX Sensortech, Switzerland) (Fig. S3). Investigations at a wide range of gas concentrations indicated that the detection had linear electrical responses, and the inset (Fig. 2c) provides a detection limit (DL) of ~20 ppb, which was estimated by a linear least squares fit for data collected at room temperature[32]. The excellent sensitivity sufficiently detects concentrations required in potential applications, such as concentrations in exhalation by asthma and halitosis patients (>100 ppb) and the atmosphere (0.6–5 ppm)[33–35]. The rationale that crystallinity, thickness, device layout, and electrical operation would affect the exceptional performance of the bioresorbable silicon devices motivated various types of examinations. Figure 2d shows the measured responses using different kinds of silicon, such as SC-Si NMs (black), polycrystalline silicon (red, p-Si), and amorphous silicon (blue, α-Si), with identical dimensions (1.45 mm × 1.2 mm) and thicknesses (~100 nm), providing evidence of a dependence on Si crystallinity (Fig. S4). Analyses of other factors, e.g., film thickness, electrode layout, and applied voltage, are shown in Fig. S5, and dissolvable metals for coplanar interdigitated electrodes (IDEs) did not affect the functional properties (Fig. S6). The selective response to specific target gases is also an important criterion. We performed selectivity assays for well-known gases: oxidizing gases such as NO_2 (black) and NO (red) and reducing gases such as NH_3 (blue), CH_3COOH_3 (green, acetone), CH_2H_3OH (magenta, ethanol), CO_2 (cyan), CO (navy), and H_2S (purple). The resulting properties in Fig. 2e indicate that the responsiveness to NO and NO_2 was at least 100-fold greater than that to other substances (detailed data in Fig. S7), which was achieved without additional physical and chemical treatments. We note that the variation in the responses between NO and NO_2 gases was negligible (see Fig. S8). The temperature dependence of the sensitivity shown in Fig. 2f was evaluated to consider potential utility as medical implants and environmental monitors (black, RT; red, 37 °C; blue, 50 °C). The results were opposite to the typical behavior of conventional gas sensors, assuming that the electrical resistance/conductance of the silicon membranes would somewhat deviate from the optimum value at increased temperatures. Integration with temperature and humidity sensors can adjust the output values of gas detectors susceptible to ambient conditions for system-level functionality. The electrical characteristics of the resistive temperature device showed a sensitivity of ~9.6 nS/°C and a temperature coefficient of ~0.006 /°C (Fig. 2g), and changes in the capacitance of the humidity component were well resolved over a wide range of relative humidities (Fig. 2h).

Mechanical stability of large-scale, flexible, and stretchable gas sensor arrays

As introduced in previous reports on deformable electronics, structures that involved device islands connected by serpentine bridges allowed devices to accommodate mechanical loads without deterioration in electrical performance[36–38]. Figure 3a represents a large-scale, biodegradable sensor array (5 × 5, 1.7 cm × 1.9 cm) deployed in a mechanically soft geometry, consisting of patterned

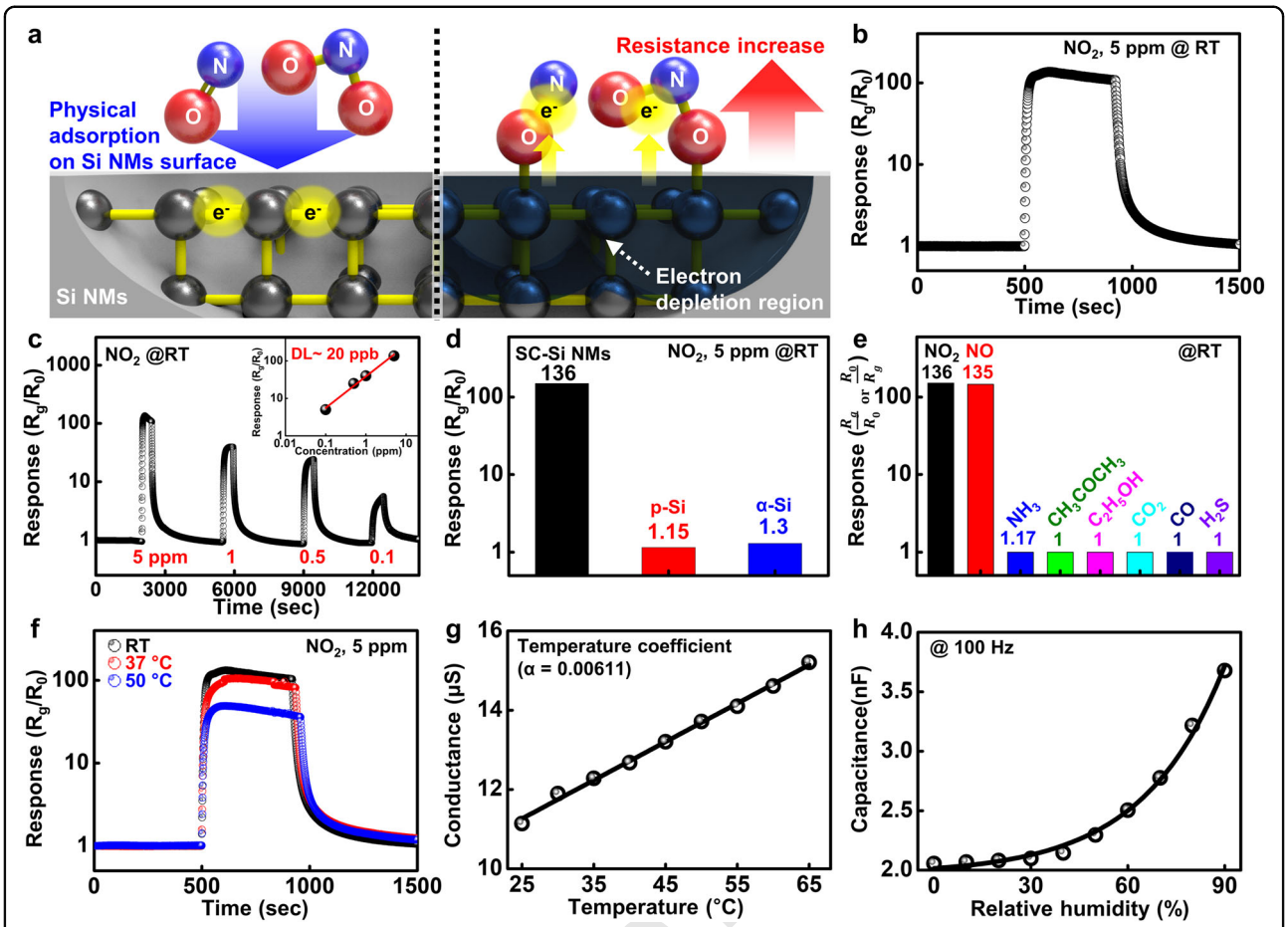

Fig. 2 High-performance bioresorbable SC-Si NM-based NO_x sensing systems. a Description of the fundamental mechanism of NO/NO_2 detection at the surface of SC-Si NMs. **b** Measured temporal response (R_g/R_0) of a biodegradable silicon-based device exposed to 5 ppm NO_2 at room temperature, showing an exceptional sensitivity of more than 100. **c** Dynamic response curves of the identical device to various concentrations of NO_2 (0.1–5 ppm) at room temperature, with an expected sensitivity limit (~20 ppb) in the inset. **d** Comparison of NO_2 detection at room temperature using several types of silicon-based materials, indicating the superior sensitivity of SC-Si NMs (black, SC-Si NMs; red, poly-Si; blue, α-Si). **e** High selectivity of the SC-Si NMs for NO/NO_2 (red/black) gases compared to those of well-known substances such as NH_3 (blue), CH_3COOH_3 (green), C_2H_3OH (magenta), CO_2 (cyan), CO (navy), and H_2S (purple). **f** Measurements of temperature-dependent responses of the SC-Si NMs to NO_2: the response rates were inversely related to temperature (black, room temperature; red, 37 °C; blue, 50 °C). **g** Measured characteristics of a temperature sensor integrated into the NO_x sensing system to adjust the effects of temperature on the gas responses. **h** Electrical measurements at various humidity levels to correct the humidity effects on measured gas values.

SC-Si NMs as active components, Mg conductors for contact pads and interconnects, patterned SiO_2 layers for interlayer dielectrics, and polycaprolactone (PCL) as substrate/encapsulant. The inset shows a magnified optical micrograph of an individual unit. Figure 3b, c show a set of images under mechanical tests using several bending radii (left, flat; middle, 5 mm; right, 3 mm) and uniaxial tensile strains up to 40%, respectively. An experimental setup combined with a stretching system is shown in Fig. S9. The resulting values under those deformed conditions remained within effective ranges of 90% (Fig. 3d, bending) and 95% (Fig. 3e, stretching). In addition, the mechanical robustness and durability of the electronic system were investigated under cyclic bending with a radius of 5 mm (black) and stretching with 35% (red), as shown in Fig. 3f, and the decreases in the relative response rate in both cases after 1000 cycles were negligible. Three-dimensional finite element analysis was implemented in the commercial ABAQUS package to study the mechanical deformation of the biodegradable Si-based gas sensor upon bending and stretching. Without losing generality, a 2 × 2 array of gas sensors was considered in the simulation, and the substrate (100 μm) and encapsulation (50 μm) layers were modeled by an 8-node 3D element (C3D8R). PCL (Young's modulus, 0.25 GPa; Poisson ratio, 0.44) and semipermeable membranes (PDMS, 2.61 MPa; 0.49) were explored for the substrate and encapsulation in the bending test (Fig. 3d),

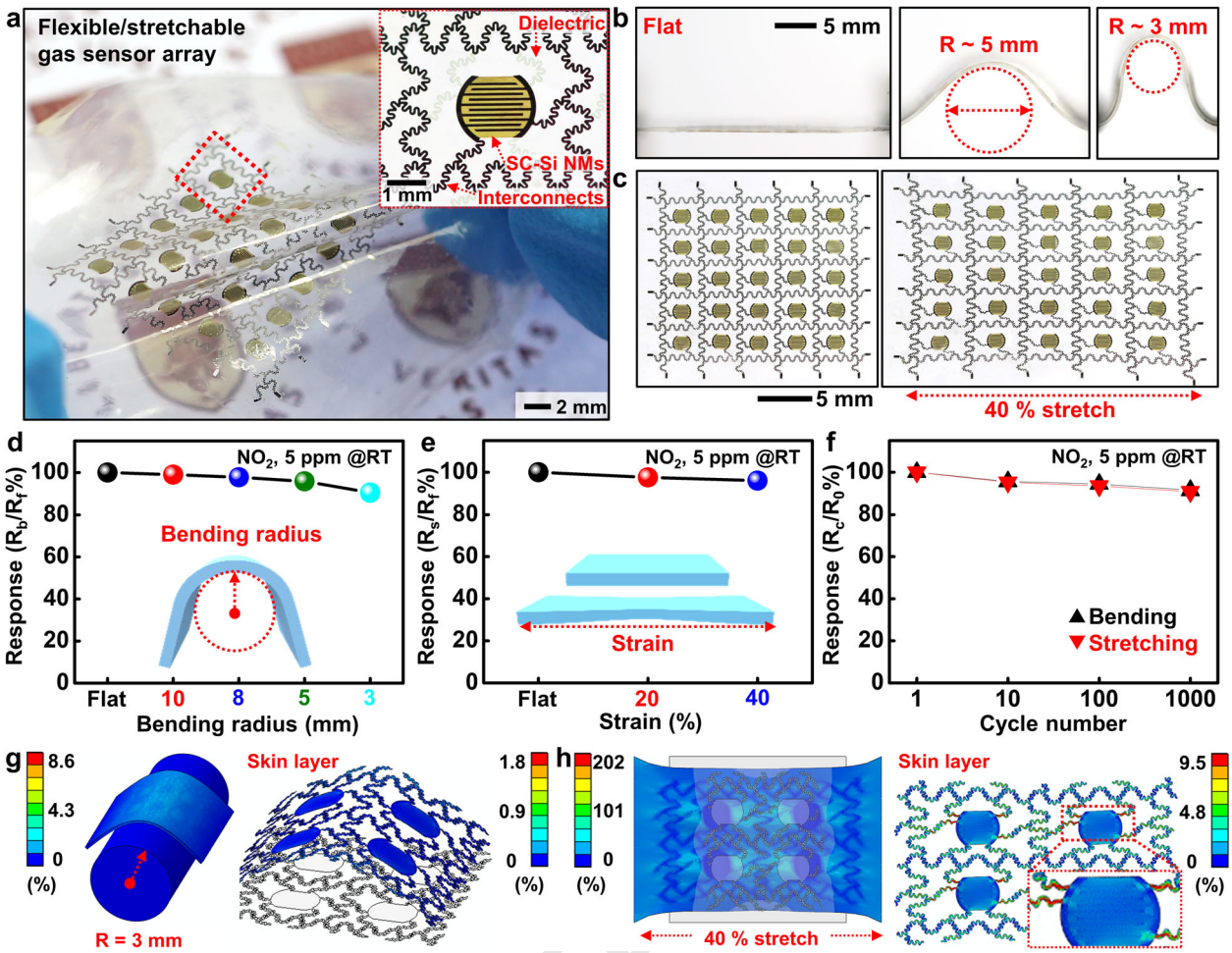

Fig. 3 Evaluations of a stretchable, dissolvable NO_x sensing system upon diverse mechanical deformations. a An array (5 × 5) of a large-scale, soft gas sensor, including a magnified device image in the inset. **b** A set of images under several bending strains (left, normal; middle, *R* ~5 mm; right, *R* ~3 mm). **c** Photographs of the devices mechanically elongated up to 40% (right). **d**, **e** Comparison of electrical characteristics of the gas detector measured at d bent states (black, flat; red, *R* ~10 mm; green, *R* ~8 mm; blue, *R* ~5 mm; cyan, *R* ~3 mm) and **e** uniaxial tensile strains (black, normal; red, 20% stretch; green, 40% stretch). **f** Investigations of the mechanical robustness of a gas sensor (black, bending; red, stretching) under cyclic bending (*R* ~5 mm, 1000 cycles) and stretching (tensile strain ~30%, 1000 cycles) conditions. **g**, **h** Theoretical analyses of the mechanical robustness and stability of the gas sensor under repetitive bending and stretching conditions. The results of the finite element method (FEM) for mechanically soft configurations designed to maintain electrical functions of the system during **g** bending and **h** stretching.

whereas PDMS was used for the substrate in the tensile test (Fig. 3e). Because of their thinness, gas-sensitive Si nanomembranes (188 GPa; 0.28), Mg electrodes and interconnects (45 GPa; 0.29), and SiO_2 interlayer dielectrics (66.3 GPa; 0.15) could be modeled as skin layers, as shown in Fig. S10. For bending with a radius of curvature of 3 mm in Fig. 3g, the maximum principal strains in the layers of Mg, SiO_2, and Si were obtained at 1.66, 1.81, and 0.24% (Fig. S11), far below their corresponding fracture strains, which explains the mechanical stability. Upon stretching, the maximum principal strain in the skin layer occurred in the serpentine interconnect near the Si nanomembrane (Fig. 3h), and detailed strain distributions for each material are shown in Fig. S11. When the total stretchability of the system is defined at a level, where the maximum principal strain of half the width of one section exceeded the fracture strain of the metal interconnect (9–10% for Mg thin film[39,40]), as in a previous report[37], the obtained total stretchability of ~40% corresponded well to the experimental value of Fig. 3e. The strain distribution in the SiO_2 layer was similar to that in the Mg layer, although the SiO_2 layer would fracture before the Mg layer due to its slightly smaller fracture strain of 8%[41]. In addition, the peak strain of 4.1% in the Si layer was immediately below its fracture strain of 4.25%[42], which explained the fracture of the Si layer upon further stretching.

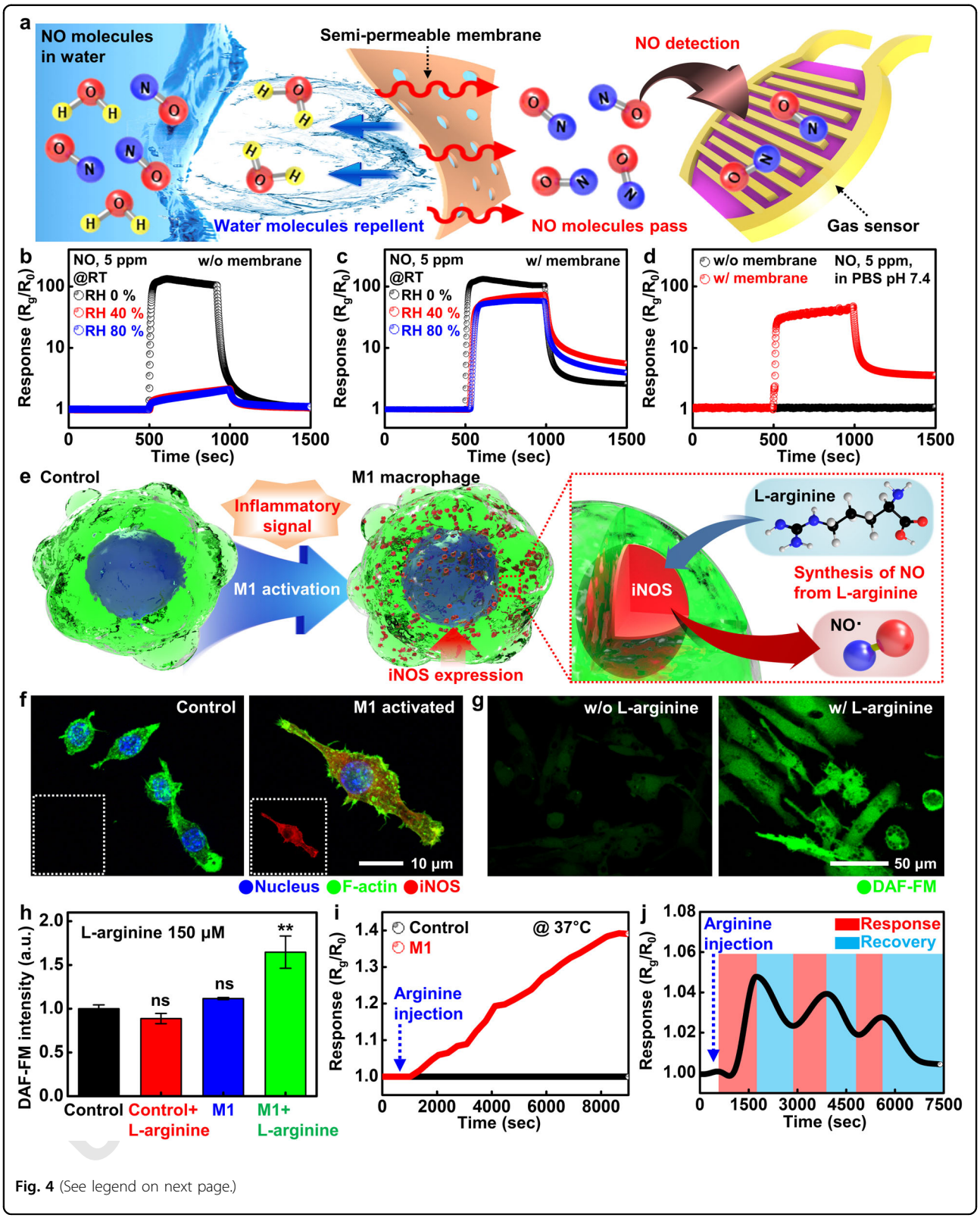

Fig. 4 (See legend on next page.)

(see figure on previous page)
Fig. 4 In vitro detection of NO produced in macrophages using transient silicon sensors with semipermeable membranes. a Schematic illustration of the principle of enabling gas measurements in humid conditions and aqueous solutions. Semipermeable membranes (polydimethylsiloxane, PDMS, thickness ~50 μm) selectively allow passage of gas molecules while acting as a barrier to water molecules. **b**, **c** Evaluations of the electrochemical responses of integrated gas sensors **b** without and **c** with a thin sheet of semipermeable membrane (thickness ~50 μm) to 5 ppm NO gas at several levels of relative humidity (black, 0%; red, 40%; blue, 80%). **d** Measured electrical properties of integrated gas sensors without (black) and with (red) semipermeable membranes in phosphate-buffered saline (PBS, pH 7.4) solution. **e** Description of key procedures for nitric oxide (NO) production through the inflammatory response of macrophages (left). The production of NO from L-arginine through enzymatic reactions by inducible nitric oxide synthase (iNOS) is shown in the inset (right). **f** Representative images of control (left) and M1-activated (right) RAW 264.7 macrophages. Nuclei (blue), F-actin (green), and iNOS (red) were visualized by maximum intensity projection of immunofluorescence confocal images. Note that iNOS expressed only M1-activated macrophages. **g** Microscopic images of NO production in M1 macrophages by L-arginine treatments (left, 0 μM; right, 150 μM). **h** Quantification of DAF-FM intensity for NO measurements. Values were normalized to the control values, and significant differences were evaluated by one-way analysis of variance (ANOVA) for each group (**$p < 0.01$, NS; $p > 0.05$). **i** In vitro experiments assessing electrical responses to NO generated from control and M1 cells after injection with 150 μM L-arginine. **j** Measured dynamic NO responses over time as periodic excitations and inhibitions.

In vitro assessments of dissolvable gas sensors using a semipermeable membrane

Humidity-free gas meters enable the maintenance of robust performance even in harsh environments in envisioned areas of interest. Figure 4a illustrates the fundamental principle that a PDMS-based semipermeable membrane can effectively deliver desired gas components to active areas of an electronic system and repel water and/or aqueous components[43,44]. The PDMS membrane provides hydrophobicity and gas permeability since methyl groups ($Si–CH_3$) on the surface of PDMS reduce the surface energy, and siloxane backbones (Si–O) inside the polymer network form a pathway for NO diffusion. In comparative experiments without (Fig. 4b) or with (Fig. 4c) membranes, absolute values of the responsiveness were slightly reduced, while the electrical characteristics still exhibited a high level of sensitivity compared to those in the tests where there were nearly no responses with even a small amount of moisture in the absence of the membrane. Similar behaviors were found during immersion in aqueous media, in which the membrane enabled stable detection in phosphate-buffered saline (PBS, pH 7.4) solution, whereas no signals were observed without the membrane (Fig. 4d and experimental setup appeared in Fig. S12). Detailed studies of the correlation between membrane thickness and system performance could enhance the sensitivity under optimized conditions (Fig. S13).

In vitro assessment of the NO detection capability indicated the feasibility of using silicon-based bioresorbable devices for applications in temporary implants. Figure 4e briefly describes the overall procedure of NO production that is recognized as a regulator of inflammatory responses in living macrophages[26]. Macrophages undergo M1 activation in response to pathogen-specific molecules, lipopolysaccharide (LPS) or proinflammatory cytokines such as TNF-α and interferon-γ (INF-γ)[45]. As a result of inflammatory activation, macrophages produce inducible nitric oxide synthase (iNOS), one of the key enzymes that acts as a catalyst to produce NO by consuming L-arginine[46]. A set of fluorescence confocal images verified the expression of iNOS, cellular morphological changes (Fig. 4f) and NO production in the presence of L-arginine (Fig. 4g). Quantitative analysis of immunofluorescence intensity is shown in Fig. S14. The produced NO reacted with DAF-FM to increase the fluorescence intensity in Fig. 4h, suggesting that both iNOS expression and the presence of L-arginine were essential factors. Figure 4i shows the measured responses after an injection of L-arginine (150 μM) into control (black) and M1-activated macrophages (red) in medium (L-arginine-free DMEM (2 ml)). Details of the experimental setup are shown in Fig. S15. The results showed that there was no response in the control group without M1 activation, while a linear response was clearly seen in the activated group, as expected. Evaluation of the dynamic response over time in Fig. 4j was performed through periodic L-arginine injections and ventilations, verifying the capability of the system for reliable and repeatable measurements of produced NO concentrations.

Conclusion

The concepts introduced here provide materials, a manufacturing strategy and device layouts for a soft, transient NO_x gas detector integrated with temperature and hydration meters. Electrical measurements reveal that the thickness, crystallinity, and operation voltage have a strong influence on the record-high sensitivity and selectivity with rapid response and recovery rates. Upon mechanical deformations by diverse modalities, the performance of large-scale arrays change negligibly, consistent with those determined by theoretical calculations. In vitro studies provide the feasibility of stable operation in harsh conditions, suggesting practical uses in environmental monitoring and biomedical implants.

Acknowledgements
This work was supported by a Korea University grant; KU-KIST Graduate School of Converging Science and Technology Program, the National Research Foundation of Korea (NRF), funded by the Ministry of Science, ICT & Future Planning (MSIP) (grant NRF-2017R1E1A1A01075027); and the Technology Innovation Program (20002974, Development of biosensing function antibiosis wound dressing and instrument for the treatment) funded by the Ministry of Trade, Industry & Energy (MOTIE, Korea). Computations for this research were performed at Pennsylvania State University's Institute for Computational and Data Sciences Advanced CyberInfrastructure (ICDS-ACI). J.Z. and H.C. also acknowledge support from the Doctoral New Investigator grant from the American Chemical Society Petroleum Research Fund (59021-DNI7) and National Science Foundation (ECCS-1933072).

Author details
[1]KU-KIST Graduate School of Converging Science and Technology, Korea University, 145 Anam-ro, Seongbuk-gu, Seoul 02841, Republic of Korea. [2]Electrical Engineering Division, Department of Engineering, University of Cambridge, 9 JJ Thomson Avenue, Cambridge CB3 0FA, UK. [3]Department of Engineering Science and Mechanics, The Pennsylvania State University, University Park, PA 16802, USA. [4]Center for Electronic Materials, Korea Institute of Science and Technology, 5, Hwarang-ro 15-gil, Seongbuk-gu, Seoul 02792, Republic of Korea

Conflict of interest
The authors declare that they have no conflict of interest.

Supplementary information is available for this paper at https://doi.org/10.1038/s41427-020-00253-0.

Received: 6 June 2020 Revised: 3 September 2020 Accepted: 15 September 2020.
Published online: xx xxx 2020

References

1. Koh, A. et al. A soft, wearable microfluidic device for the capture, storage, and colorimetric sensing of sweat. *Sci. Transl. Med.* **8**, 366ra165–366ra165 (2016).
2. Gao, W. et al. A fully integrated wearable sensor arrays for multiplexed in situ perspiration analysis. *Nature* **529**, 509–514 (2016).
3. Yang, Y. et al. A laser-engraved wearable sensor for sensitive detection of uric acid and tyrosine in sweat. *Nat. Biotechnol.* **38**, 217–224 (2020).
4. Kaltenbrunner, M. et al. An ultra-lightweight design for imperceptible plastic electronics. *Nature* **499**, 458–463 (2013).
5. Yu, X. et al. Skin-integrated wireless haptic interfaces for virtual and augmented reality. *Nature* **575**, 473–479 (2019).
6. Tee, B. C.-K., Wang, C., Allen, R. & Bao, Z. An electrically and mechanically self-healing composite with pressure-and flexion-sensitive properties for electronic skin applications. *Nat. Nanotechnol.* **7**, 825 (2012).
7. Huang, Y. et al. A self-healable and highly stretchable supercapacitor based on a dual crosslinked polyelectrolyte. *Nat. commun.* **6**, 1–8 (2015).
8. Kim, T. I. et al. Injectable, cellular-scale optoelectronics with applications for wireless optogenetics. *Science* **340**, 211–216 (2013).
9. Jeong, J.-W. et al. Wireless optofluidic systems for programmable in vivo pharmacology and optogenetics. *Cell* **162**, 662–674 (2015).
10. Yu, K. J. et al. Bioresorbable silicon electronics for transient spatiotemporal mapping of electrical activity from the cerebral cortex. *Nat. Mater.* **15**, 782–791 (2016).
11. Kang, S.-K. et al. Bioresorbable silicon electronic sensors for the brain. *Nature* **530**, 71–76 (2016).
12. Koo, J. et al. Wireless bioresorbable electronic system enables sustained non-pharmacological neuroregenerative therapy. *Nat. Med.* **24**, 1830–1836 (2018).
13. Kim, H.-S. et al. Bioresorbable silicon nanomembranes and iron catalyst nanoparticles for flexible, transient electrochemical dopamine monitors. *Adv. Healthc. Mater.* **7**, 1801071 (2018).
14. Guzik, T. J., West, N. E. J., Pillai, R., Taggart, D. P. & Channon, K. M. Nitric oxide modulates superoxide release and peroxynitrite formation in human blood vessels. *Hypertension* **39**, 1088–1094 (2002).
15. Farah, C., Michel, L. Y. M. & Balligand, J.-L. Nitric oxide signalling in cardiovascular health and disease. *Nat. Rev. Cardiol.* **15**, 292–316 (2018).
16. Wennberg, P. O. & Dabdub, D. Rethinking ozone production. *Science* **319**, 1624–1625 (2008).
17. Li, S., Matthews, J. & Sinha, A. Atmospheric hydroxyl radical Production from electronically excited NO_2 and H_2O. *Science* **319**, 1657–1660 (2009).
18. Liu, S., Wang, Z., Zhang, Y., Zhang, C. & Zhang, T. High performance room temperature NO_2 sensors based on reduced graphene oxide-multiwalled carbon nanotubes-tin oxide nanoparticles hybrids. *Sens. Actuators B* **211**, 318–324 (2015).
19. Wang, Z., Huang, L., Zhu, X., Zhou, X. & Chi, L. An ultra-sensitive organic semiconductor NO_2 sensor based on crystalline TIPS-pentacene films. *Adv. Mater.* **29**, 1703192 (2017).
20. Sahu, P. K., Pandey, R. K., Dwivedi, E., Mishra, V. N. & Prakash, R. Polymer/Graphene oxide nanocomposite thin film for NO_2 sensor: an in situ investigation of electronic, morphological, structural, and spectroscopic properties. *Sci. Rep.* **10**, 2981 (2020).
21. Peng, K.-Q., Wang, X. & Lee, S.-T. Gas sensing properties of single crystalline porous silicon nanowires. *Appl. Phys. Lett.* **95**, 243112 (2009).
22. Yan, W., Hu, M., Wang, D. & Li, C. Room temperature gas sensing properties of porous silicon/V_2O_5 nanorods composite. *Appl. Surf. Sci.* **346**, 216–222 (2015).
23. Moon, H. G. et al. Glancing angle deposited WO_3 nanostructures for enhanced sensitivity and selectivity to NO_2 in gas mixture. *Sens. Actuators B Chem.* **229**, 92–99 (2016).
24. Zheng, X. & Cheng, H. Y. Flexible and stretchable metal oxide gas sensors for healthcare. *Sci. China Technol. Sci.* **62**, 209–223 (2019).
25. Yang, L. et al. Novel gas sensing platform based on a stretchable laser-induced graphene pattern with self-heating capabilities. *J. Mater. Chem. A* **8**, 6487–6500 (2020).
26. Bogdan, C. Nitric oxide and the immune response. *Nat. Rev. Immunol.* **2**, 907–916 (2001).
27. Calabrese, V. et al. Nitric oxide in the central nervous system: neuroprotection versus neurotoxicity. *Nat. Rev. Neurosci.* **8**, 767–775 (2007).
28. Moon, H. G. et al. All villi-like metal oxide nanostructures-based chemiresistive electronic nose for an exhaled breath analyzer. *Sens. Actuators B* **257**, 295–302 (2018).
29. Hwang, S.-W. et al. A physically transient form of silicon electronics. *Science* **337**, 1640–1644 (2012).
30. Kang, S.-K. et al. Dissolution behaviors and applications of silicon oxides and nitrides in transient electronics. *Adv. Funct. Mater.* **24**, 4427–4434 (2014).
31. Hwang, S.-W. et al. High-performance biodegradable/transient electronics on biode-gradable polymers. *Adv. Mater.* **26**, 3905–3911 (2014).
32. Long, G. L. & Winefordner, J. D. Limit of detection. A closer look at the IUPAC definition. *Anal. Chem.* **55**, 712A–724A (1983).
33. Ricciardolo, F. L. M., Sterk, P. J., Gaston, B. & Folkerts, G. Nitric oxide in health and disease of the respiratory system. *Physiol. Rev.* **84**, 731–765 (2004).
34. Hesterberg, T. W. et al. Critical review of the human data on short-term nitrogen dioxide (NO_2) exposures: evidence for NO_2 no-effect levels. *Crit. Rev. Toxicol.* **39**, 743–781 (2009).
35. Council, N. R. *Assessment of Exposure-Response Functions for Rocket-Emission Toxicants*. (National Academies Press, Washington, 1998) 147–162.
36. Kim, D.-H. et al. Epidermal electronics. *Science* **333**, 838–843 (2011).
37. Fan, J. A. et al. Fractal design concepts for stretchable electronics. *Nat. Commun* **5**, 3266 (2014).
38. Hwang, S.-W. et al. Biodegradable elastomers and silicon nanomembranes/nanoribbons for stretchable, transient electronics, and biosensors. *Nano Lett.* **15**, 2801–2808 (2014).
39. Somekawa, H. & Mukai, T. Effect of grain refinement on fracture toughness in extruded pure magnesium. *Scr. Mater.* **53**, 1059–1064 (2005).
40. Jessen, L. K., Zamponi, C. & Quandt, E. Mechanical properties of magnetron sputtered free standing Mg-Ag alloy films. *Front. Mater.* **6**, 236 (2019).
41. Mačović, M. et al. A novel approach for preparation and in situ tensile testing of silica glass membranes in the transmission electron microscope. *Front. Mater.* **4**, 10 (2017).
42. Ando, T., Shikida, M. & Sato, K. Tensile-mode fatigue testing of silicon films as structural materials for MEMS. *Sens. Actuators A* **93**, 70–75 (2001).
43. Kim, R.-H. et al. Waterproof AlInGaP optoelectronics on stretchable substrates with applications in biomedicine and robotics. *Nat. Mater.* **9**, 929–937 (2010).

44. Wolf, M. P., Salieb-Beugelaar, G. B. & Hunziker, P. PDMS with designer functionalities properties, modifications strategies, and applications. *Prog. Polym. Sci.* **83**, 97–134 (2018).
45. Martinez, F. O. & Gordon, S. The M1 and M2 paradigm of macrophage activation: time for reassessment. *F1000Prime Rep.* **6**, 13 (2014).
46. Aktan, F. iNOS-mediated nitric oxide production and its regulation. *Life Sci.* **75**, 639–653 (2004).

Graphical Abstract

Soft, transient silicon-based gas sensing system capable of detecting nitrogen oxides with remarkable sensitivity and selectivity is presented in this report. The results provide materials, device layouts, manufacturing process, and theorectical modeling illlustrating the capabilities and operational aspects. In vitro experiments demonstrate the possibilities for disposable environmental monitors and temporary biomedical implants.

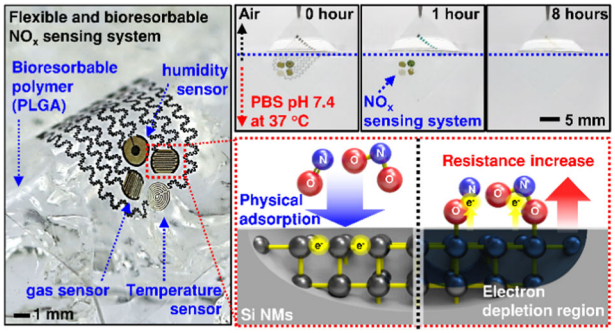

QUERY FORM

NPGASIAMATER	
Manuscript ID	**[Art. Id: 253]**
Author	
Editor	
Publisher	

Journal: NPGASIAMATER

Author :- The following queries have arisen during the editing of your manuscript. Please answer by making the requisite corrections directly in the e.proofing tool rather than marking them up on the PDF. This will ensure that your corrections are incorporated accurately and that your paper is published as quickly as possible.

Query No.	Description	Author's Response
AQ1	Please check your article carefully, coordinate with any co-authors and enter all final edits clearly in the eproof, remembering to save frequently. Once corrections are submitted, we cannot routinely make further changes to the article.	
AQ2	Author surnames have been highlighted. Please check these carefully and adjust if the first name or surname is marked up incorrectly. Note that changes here will affect indexing of your article in public repositories such as PubMed. Also, carefully check the spelling and numbering of all author names and affiliations, and the corresponding email address(es).	
AQ3	You cannot alter accepted Supplementary Information files except for critical changes to scientific content. If you do resupply any files, please also provide a brief (but complete) list of changes. If these are not considered scientific changes, any altered Supplementary files will not be used, only the originally accepted version will be published.	
AQ4	Figure 1 has panel 'a', but the panels are not mentioned in the legend. Please describe the panel, if appropriate.	